

Supporting Information

Hydrophobized Electrospun Nanofibers of Hierarchical Porosity as the Integral Gas Diffusion Electrode for Full-pH CO₂ Electroreduction in Membrane Electrode Assemblies

Min Wang, Ling Lin, Zhangyi Zheng, Zhenyang Jiao, Guowei Wang, Xiaoxing Ke, Yuebin Lian, Fenglei Lyu,* Jun Zhong, Zhao Deng, and Yang Peng*

E-mail: flly@suda.edu.cn (F.L.); ypeng@suda.edu.cn (Y.P.)

Experimental Section

Materials

Zinc nitrate hexahydrate (Zn(NO₃)₂·6H₂O, AR), nickel nitrate hexahydrate (Ni(NO₃)₂·6H₂O, AR), iridium chloride (IrCl₃) were purchased from Macklin. 2-methylimidazole, hexadecyl trimethyl ammonium bromide (CTAB), polytetrafluoroethylene (PTFE) dispersion (60 wt%) were purchased from Aladdin. Polyacrylonitrile (PAN, 200000) was purchased from Polysciences. Potassium hydroxide (KOH, ≥95%), acetone and N, N-Dimethylformamide were purchased from Sinopharm Chemical Reagent. Carbon gas diffusion electrode (YLS-30T) was obtained from Suzhou Siner technology. All materials were used as received without further purification.

Synthesis of NiZn-ZIF and NiNC-1100

Ni(NO₃)₂·6H₂O (0.12 g) and Zn(NO₃)₂·6H₂O (0.362 g) were dissolved in deionized water (12.5 mL) with stirring and poured into an aqueous solution (87.5 mL deionized water) containing 2-methylimidazole (5.67 g) and CTAB (0.025 g). After stirring for 5 min, the mixture was aged at 30 °C for 3 h. The product was collected by centrifugation and then washed by acetone and DMF. Finally, NiZn-ZIF was dried at 90 °C for 12 h in a vacuum oven. Ni-NC was obtained by pyrolysis of NiZn-ZIF under argon at 1100

°C for 2 hours.

Synthesis of NiNF-1100 membrane

PAN (1.2 g), NiZn-ZIF (1.5 g) and CNT (0.185 g) were dispersed in DMF (18 g) by ball milling for 6 h. The dispersion was then electrospun into nanofiber membrane (ZIF/CNT/PAN) at 21 kV with an injecting rate of 0.02 mL/min. ZIF/CNT/PAN was dried at 60 °C in vacuum oven overnight. ZIF/CNT/PAN was pre-oxidated in air at 240 °C for 1 hour and then calcined under argon at 1100 °C for 2 hours. The calcined membrane was soaked into 2wt% PTFE solution and heat-treated 330 °C for 1 h under argon. NiNF-900 and NiNF-1000 was prepared by the same procedure as NiNF-1100, except that they were calcined at 900 °C and 1000 °C, respectively.

Fabrication of the IrO₂/Ti electrode

Titanium mesh (2.5 cm × 2.5 cm) was treated in oxalic acid (0.5 mol L⁻¹) for 1 h to remove surface oxide layer. After washed with water and ethanol, titanium mesh was soaked in IrCl₃/isopropanol solution (30 mg/10 mL) containing 10% HCl for 5 min, dried at 100 °C for 10 min and calcinated in air at 500 °C for 30 min. The soaking procedure was repeated until the loading of IrO₂ on the titanium mesh reached 1 mg cm⁻².

Material characterization

The morphology characterizations were carried out in scanning electron microanalyzer (SEM, FEI) at an accelerating voltage of 10 KV and transmission electron microscopy (TEM, G20) at an accelerating voltage of 200 KV. XRD patterns were collected on Bruker D8 Advance X-ray with scanning speed of 1.5° min⁻¹. Raman spectra were obtained in Horiba Confocal Raman Spectroscopy. The surface chemistry was analyzed by X-ray photoelectron spectrometer (XPS, Thermo Fisher, Escalab 250Xi) with Al K α radiation. The amount of Ni was quantified by ICP-OES with an OPTIMA 8000 analyzer (PerkinElmer Inc.). N₂ and CO₂ adsorption-desorption isothermal curves were collected on the Micromeritics ASAP 2460. Ni K-edge X-ray absorption spectroscopy (XAS) was collected at Beamline 11B in Shanghai Synchrotron Radiation Facility (SSRF).

Electrochemical measurements

CO₂ electroreduction reaction were performed in a three-chamber flow cell in which the anode and cathode chamber was separated by anion exchange membrane (Fumasep FAB-PK-130). NiNF, nickel foam and Ag/AgCl (saturated KCl) were used as working electrode, counter electrode, and reference electrode electrolyte, respectively. High purity CO₂ with a constant flow rate of 30 mL min⁻¹ were supplied to the gas chamber. In the alkaline flow cell, 1 M KOH with a flow rate of 20 ml min⁻¹ was used as cathode and anode electrolyte. In the acidic flow cell, cathode and anode electrolyte were H₂SO₄/K₂SO₄ (pH = 2, C_{K⁺} = 0.5 M) and 0.5 M H₂SO₄, respectively. The internal resistance of the flow cell was measured by electrochemical impedance spectroscopy under open circuit conditions, and 85% ohmic correction was performed during the measurement. Gas products were quantitatively analyzed using gas chromatography equipped with both flame ionization and thermal conductivity detectors (Agilent 7890B). All the potentials were converted to the potentials referring to the RHE, according the following equation.

$$E_{\text{RHE}} = E_{\text{Ag/AgCl}} + 0.059\text{pH} + 0.198 + 0.85iR$$

The turnover frequency (TOF, h⁻¹) for CO was calculated as follow:¹

$$\text{TOF}(h^{-1}) = \frac{\frac{I_{\text{CO}}}{nF}}{m_{\text{cat}} * \frac{w}{M_{\text{Ni}}}} \times 3600$$

where I_{CO} is the partial current for CO. m_{cat} is the mass of catalyst on the electrode. w represents the metal loading in the catalyst based on ICP result. M_{Ni} is the atomic mass of Ni. n is the number of electrons required to form a molecule of CO. F is the Faraday constant (96485 C mol⁻¹).

For the neutral MEA test, NiNF-1100 cathode and IrO₂/Ti anode were separated an anion-exchange membrane (Sustainion X37, Dioxide Materials). A gas flow channel supplied 60 sccm humidified CO₂ while the anode was circulated with 0.1 M KHCO₃ electrolyte with a flow rate of 5 mL min⁻¹. The cell voltages were recorded without iR correction. For the acidic MEA test, NiNF-1100 cathode and IrO₂/Ti anode were separated by a cation-exchange membrane (Nafion HP). A gas flow channel supplied

humidified CO₂ (60 mL min⁻¹) while the anode was circulated with H₂SO₄/K₂SO₄ (pH = 2, C_{K⁺} = 0.1 M) electrolyte with a flow rate of 5 mL min⁻¹. The cell voltages were recorded without iR correction.

Full cell energy efficiency in MEA is calculated by the following equation:²

$$EE_{full-cell} = \frac{(1.23 + (-E_{CO}))}{-E_{full-cell}} \times FE_{CO}$$

where E_{full-cell} is the full-cell voltage applied in the MEA system.

Supporting figures

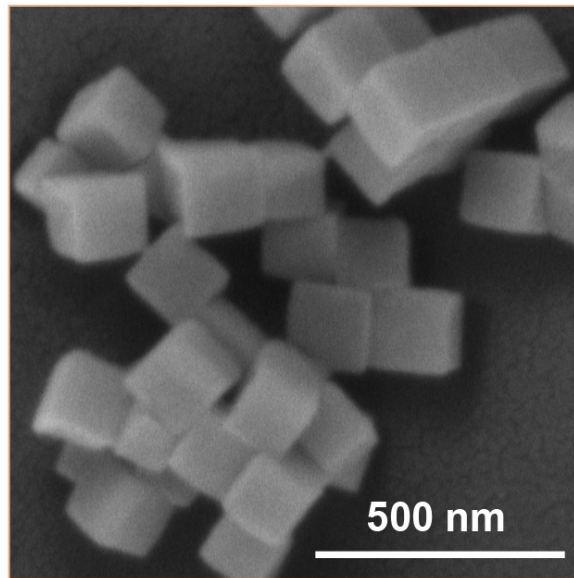


Figure S1. SEM image of NiZn-ZIF.

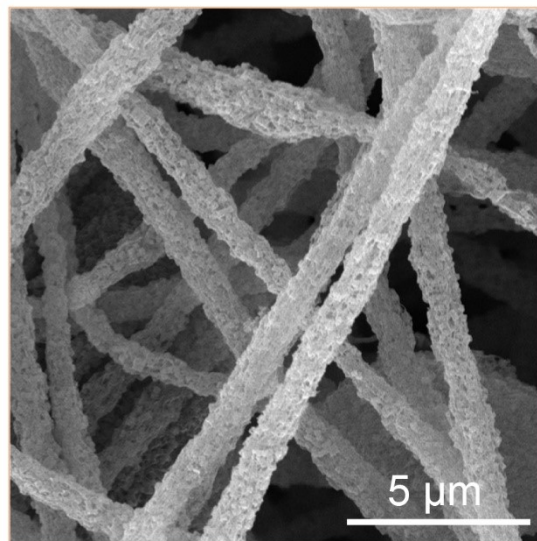


Figure S2. SEM image of ZIF/CNT/PAN.

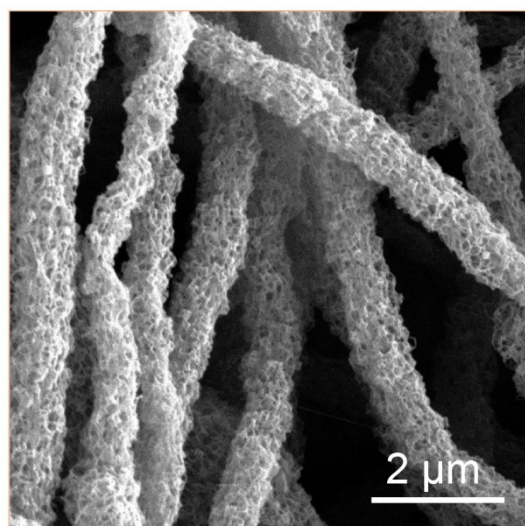


Figure S3. SEM image of pre-oxidized ZIF/CNT/PAN at 240 °C.

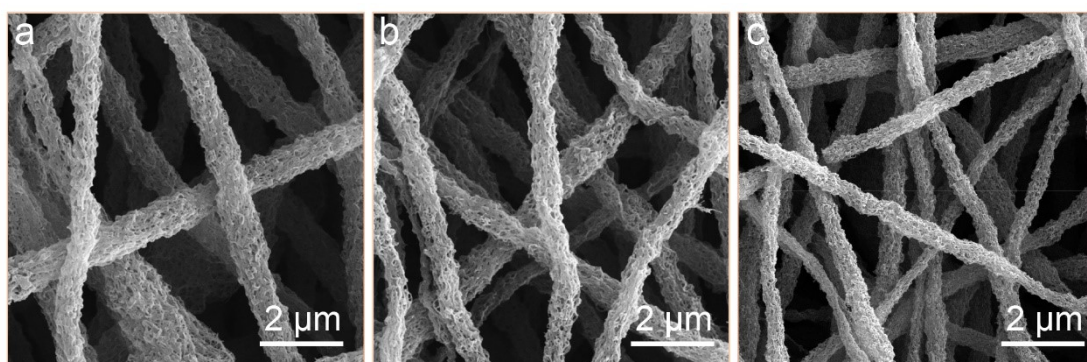


Figure S4. SEM images of (a) NiNF-900, (b) NiNF-1000 and (c) NiNF-1100.



Figure S5. Photographs illustrating the flexibility of NiNF-1100.

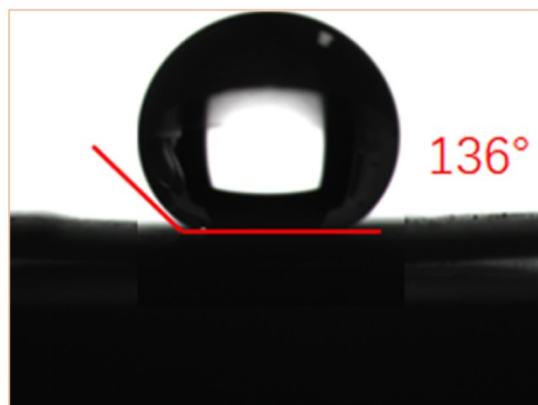


Figure S6. Contact angle of hydrophobic NiNF-1100 GDE.

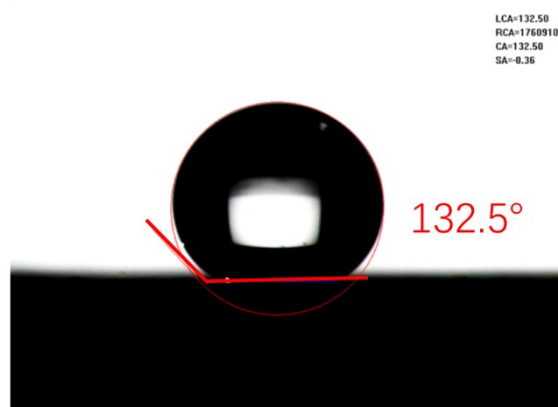


Figure S7. Contact angle of commercial YLS-30T GDE.

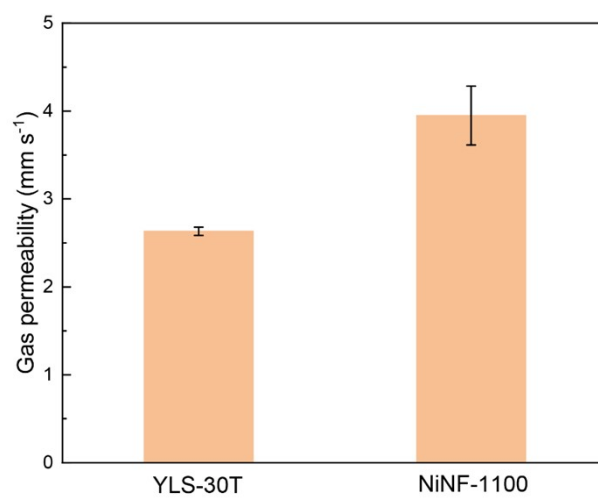


Figure S8. Gas permeability of commercial YLS-30T GDE and NiNF-1100.

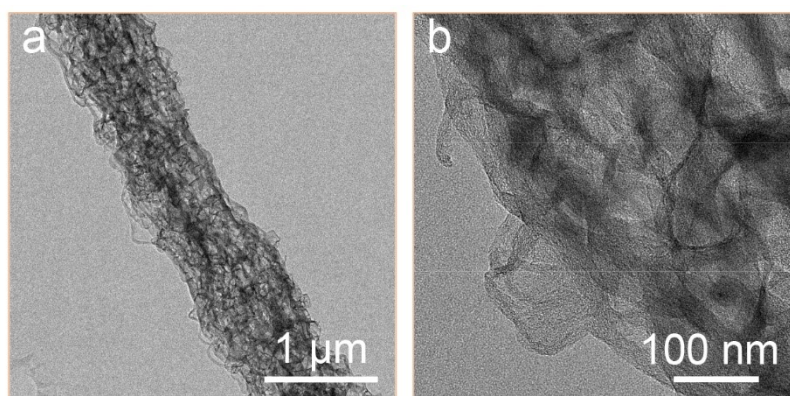


Figure S9. TEM images of NiNF-1100 at different magnifications.

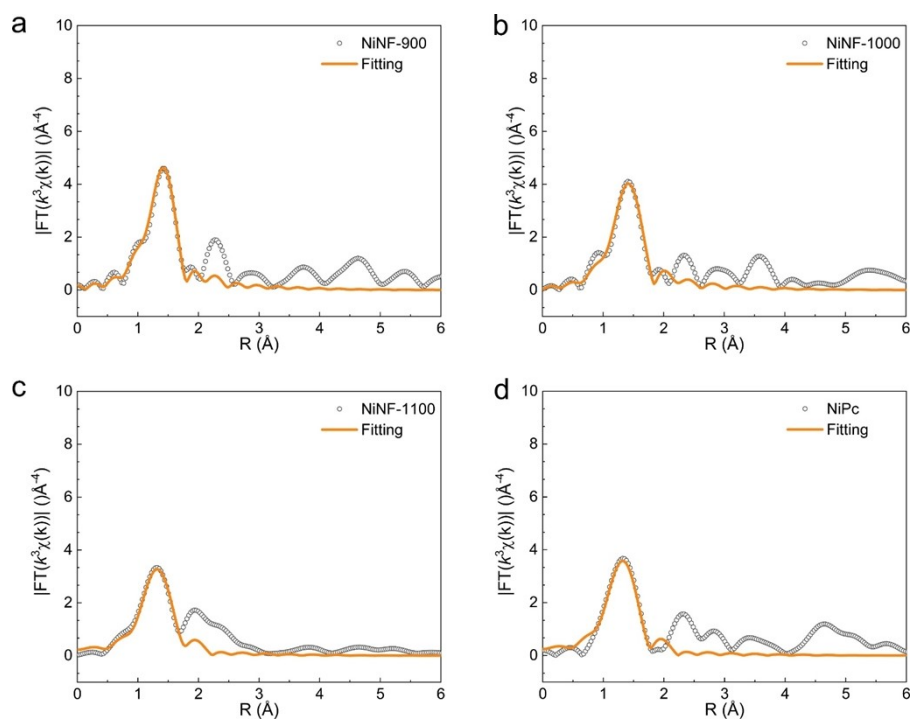


Figure S10. Fitting of the NiNF-900, NiNF-1000, NiNF-1100 and NiPc EXAFS spectra to quantify the Ni-N coordination number.

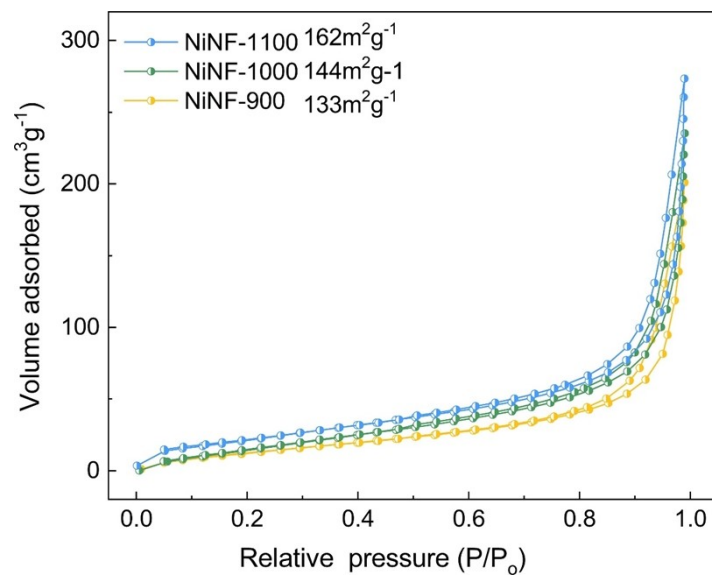


Figure S11. N_2 adsorption-desorption isotherms of NiNF-900, NiNF-1000 and NiNF-1100.

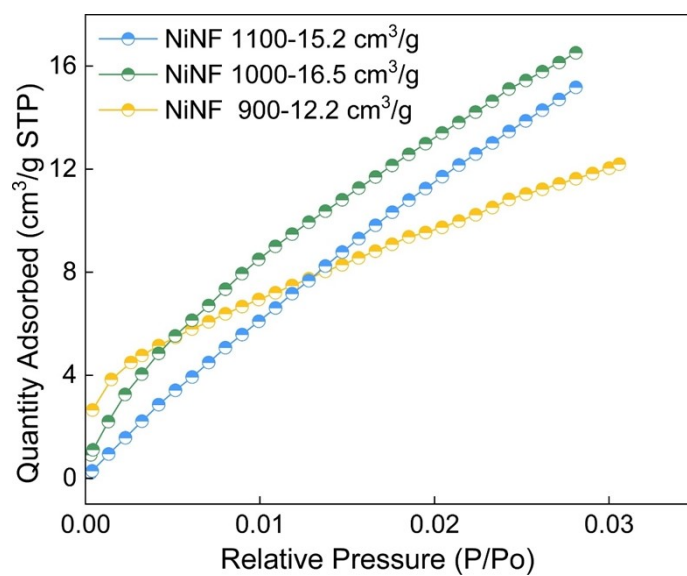


Figure S12. CO_2 uptakes of NiNF-900, NiNF-1000 and NiNF-1100.

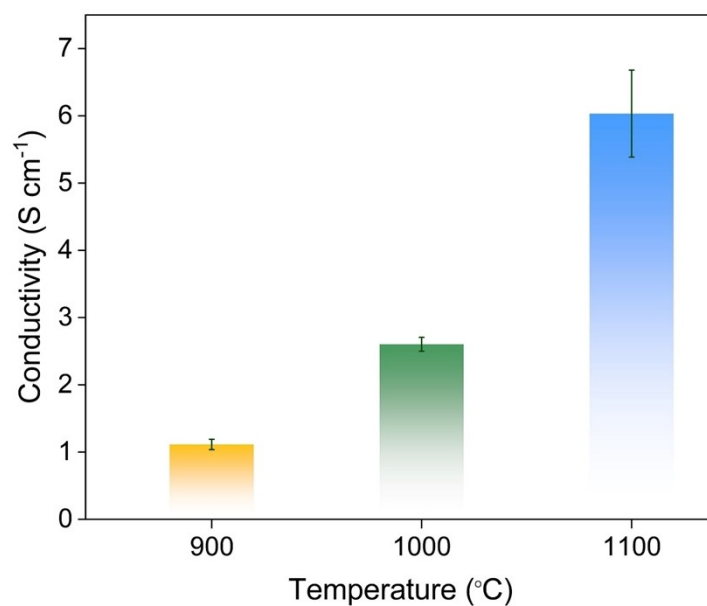


Figure S13. The conductivity of the self-standing NiNF-900, NiNF-1000 and NiNF-1100 samples.

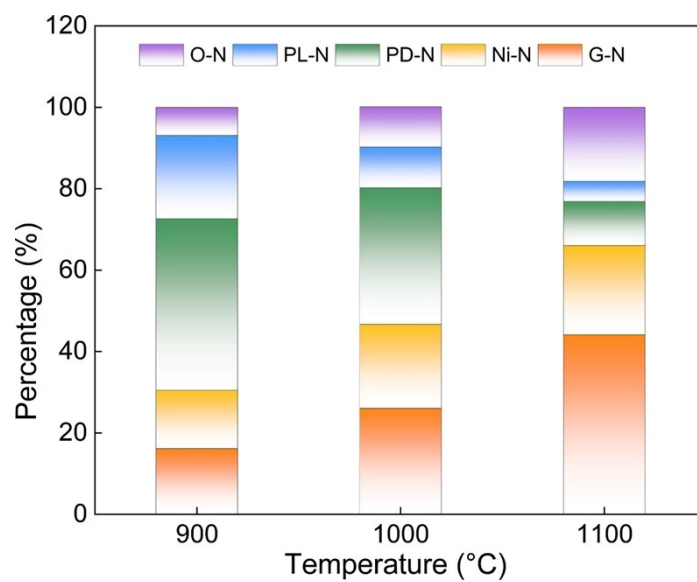


Figure S14. The contents of different N species in NiNF-900, NiNF-1000 and NiNF-1100. O-N, PL-N, PD-N, Ni-N and G-N represent oxidized N, pyrrolic N, pyridinic N, Ni-N, and graphitic N, respectively.

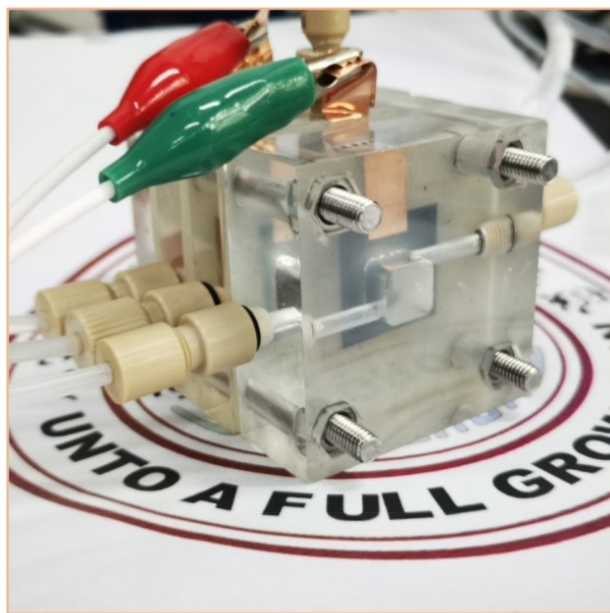


Figure S15. Photograph of a typical flow cell.

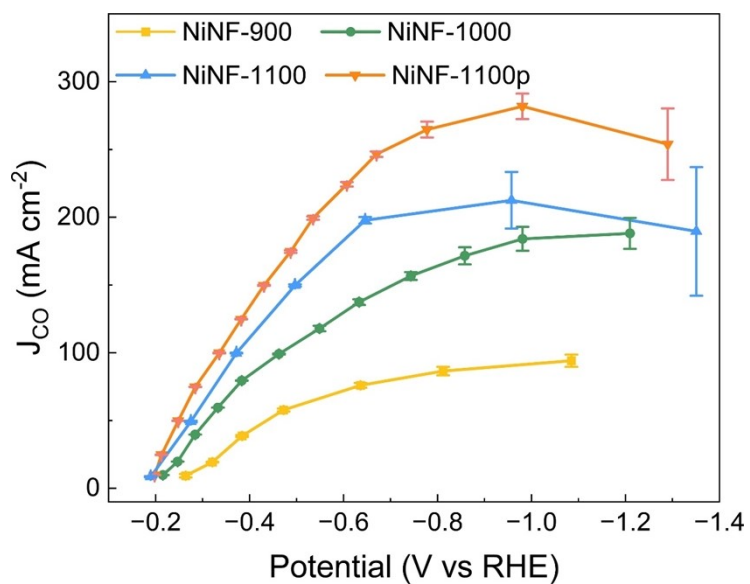


Figure S16. CO partial current density of NiNF-900, NiNF-1000, NiNF-1100 and NiNF-1100p in 1 M KOH.

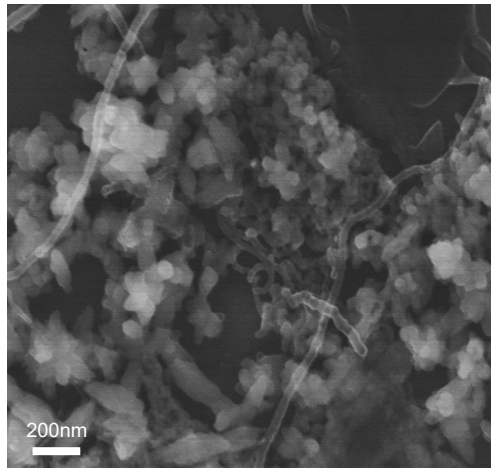


Figure S17. SEM image of NiNC-1100.

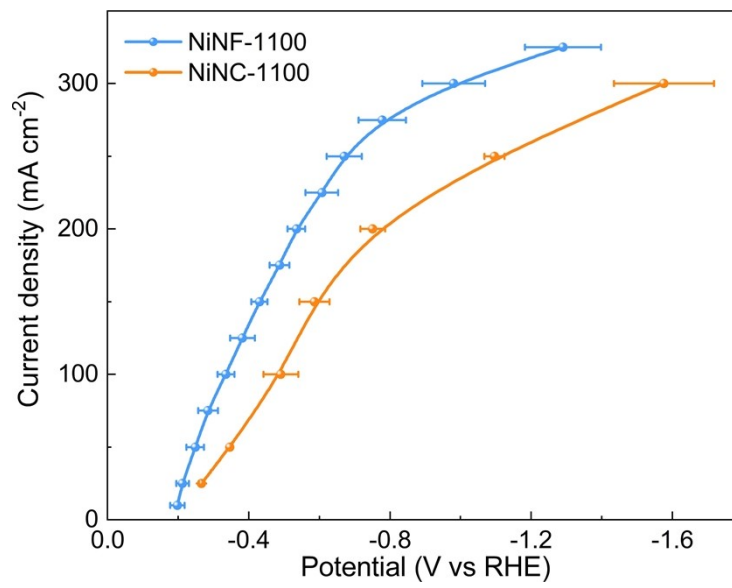


Figure S18. j-V plots of NiNF-1100 and NiNC-1100 in 1 M KOH.

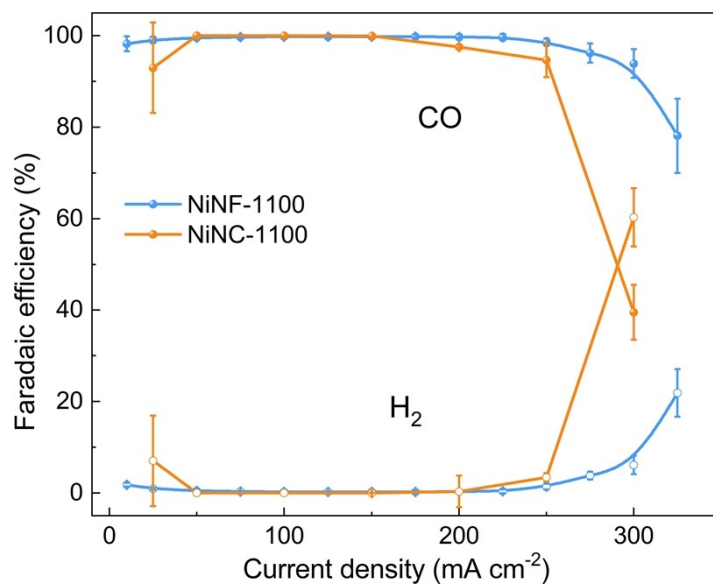


Figure S19. Faradaic efficiency of CO and H₂ for NiNF-1100 and NiNC-1100 in 1 M KOH.

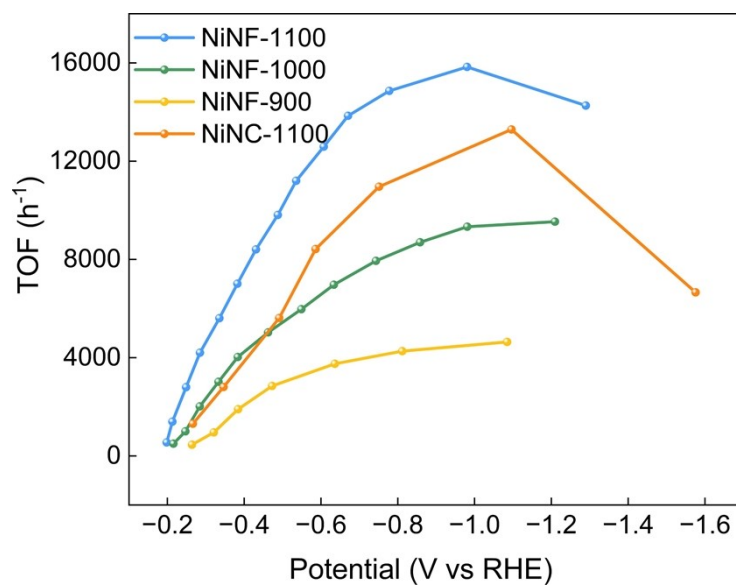


Figure S20. The TOF of NiNF-900, NiNF-1000, NiNF-1100, NiNC-1100 in 1 M KOH.

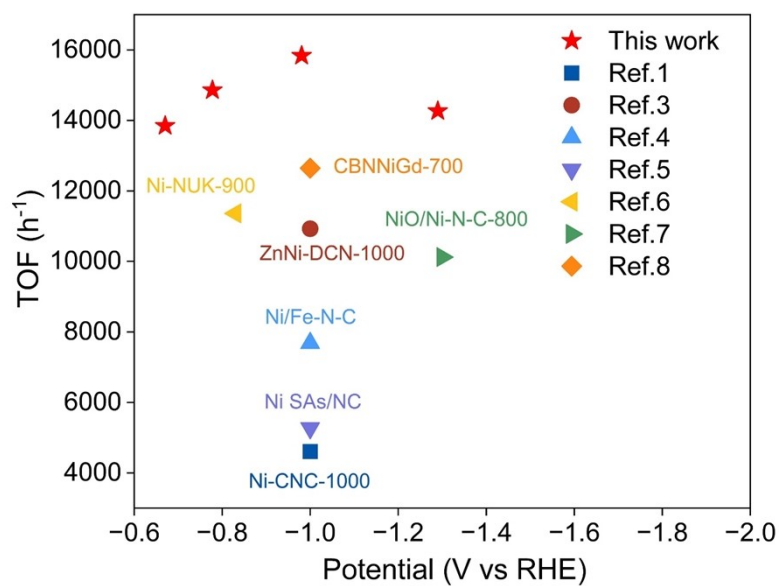


Figure S21. Comparison of TOF for NiNF-1100 with other state-of-the-art CO₂RR to CO electrocatalysts.

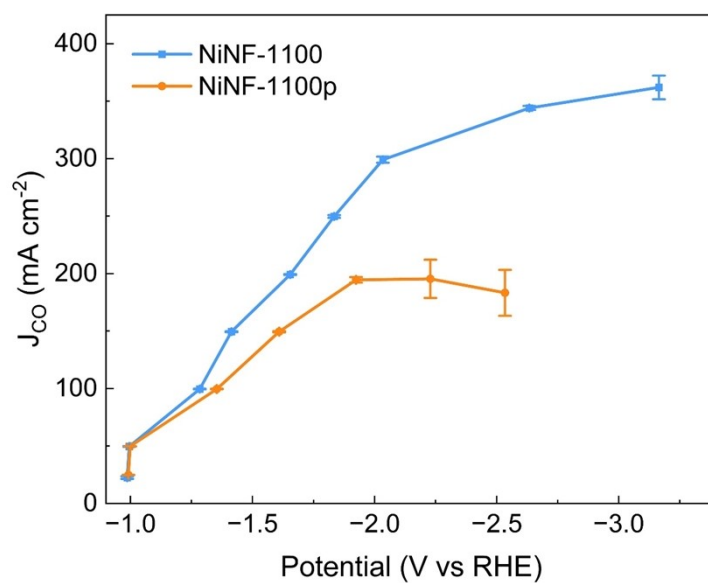


Figure S22. CO partial current density of NiNF-1100 and NiNF-1100p in H₂SO₄/K₂SO₄ (pH = 2, C_{K⁺} = 0.5 M).

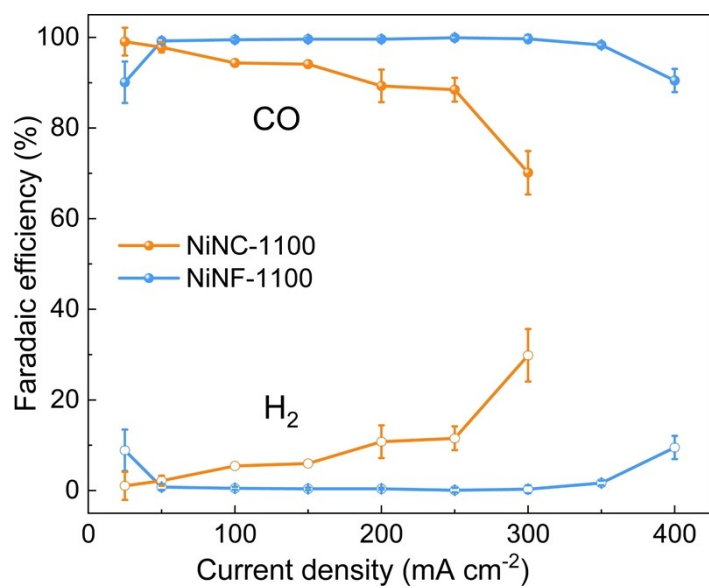


Figure S23. Faradaic efficiency of CO and H₂ for NiNF-1100 and NiNC-1100 in H₂SO₄/K₂SO₄ (pH = 2, C_{K⁺} = 0.5 M).

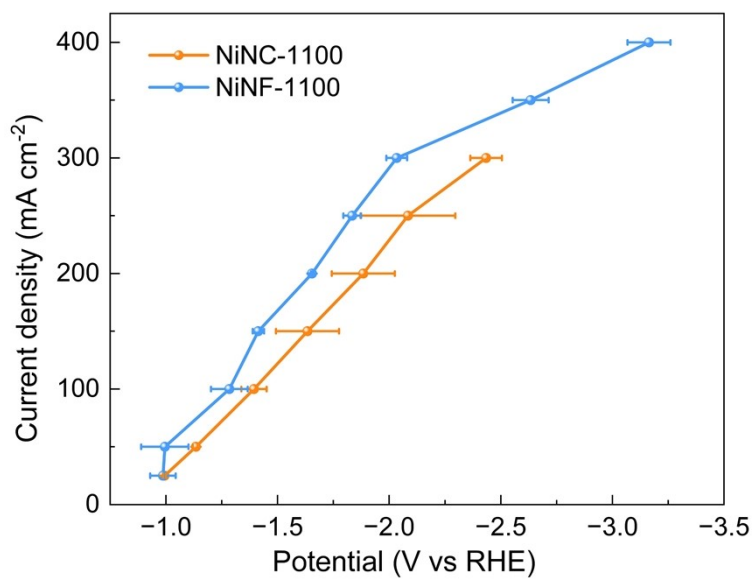


Figure S24. j-V plots of NiNF-1100 and NiNC-1100 in H₂SO₄/K₂SO₄ (pH = 2, C_{K⁺} = 0.5 M).

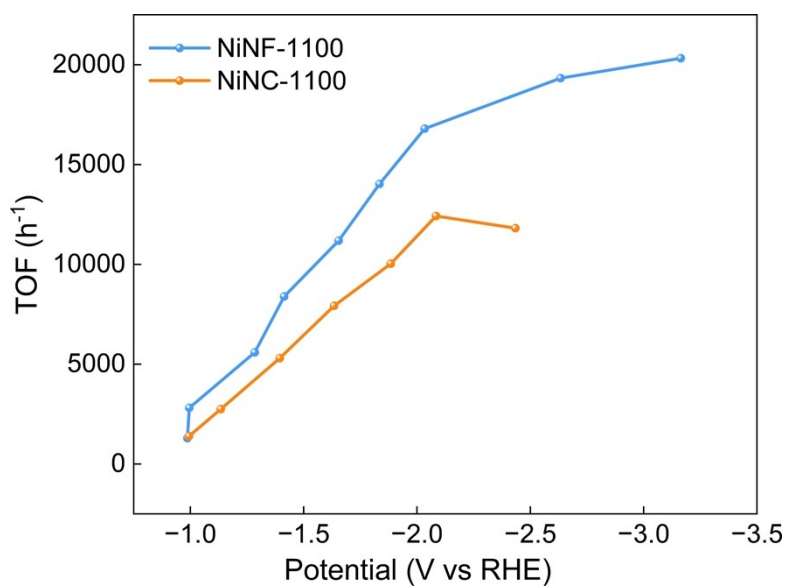


Figure S25. The TOF of NiNF-1100, NiNC-1100 in $\text{H}_2\text{SO}_4/\text{K}_2\text{SO}_4$ ($\text{pH} = 2$, $C_{\text{K}^+} = 0.5$ M).



Figure S26. Photograph of a typical MEA electrolyzer with an effective electrode area of 5 cm^2 .

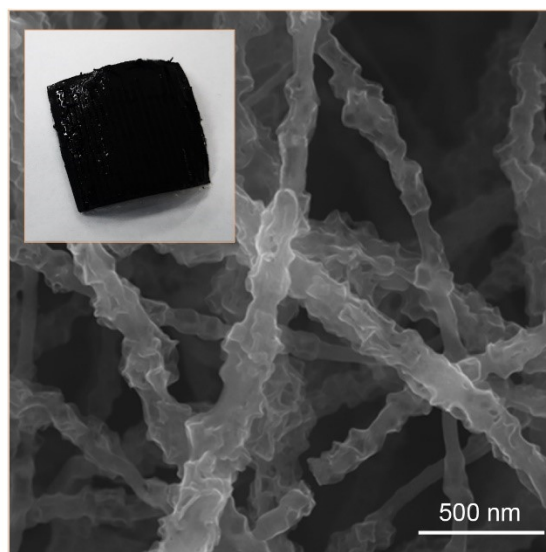


Figure S27. SEM image and photo (inset) of post-catalytic NiNF-1100 in the neutral MEA.

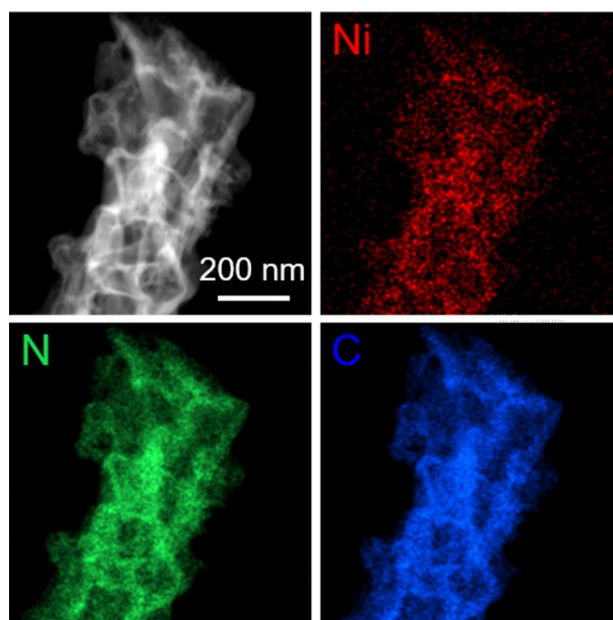


Figure S28. Elemental maps of Ni, N and C for post-catalytic NiNF-1100 in the neutral MEA.

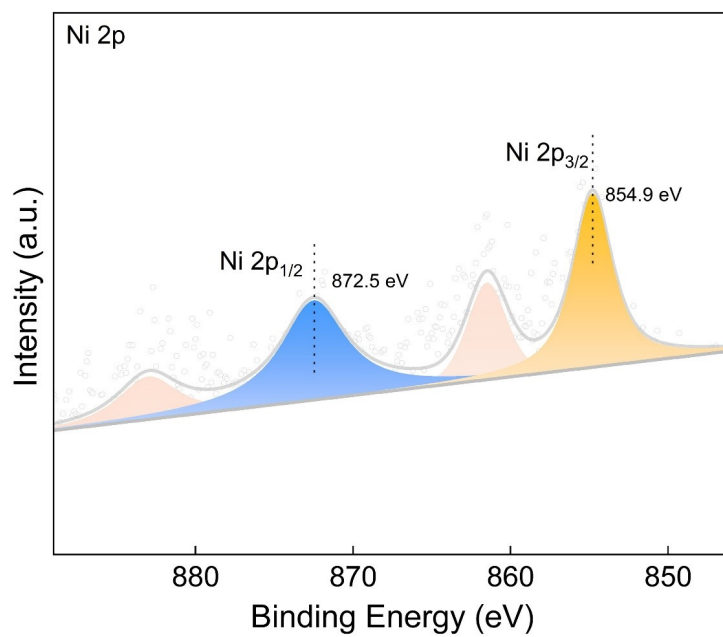


Figure S29. XPS Ni 2p spectrum of post-catalytic NiNF-1100 in the neutral MEA.

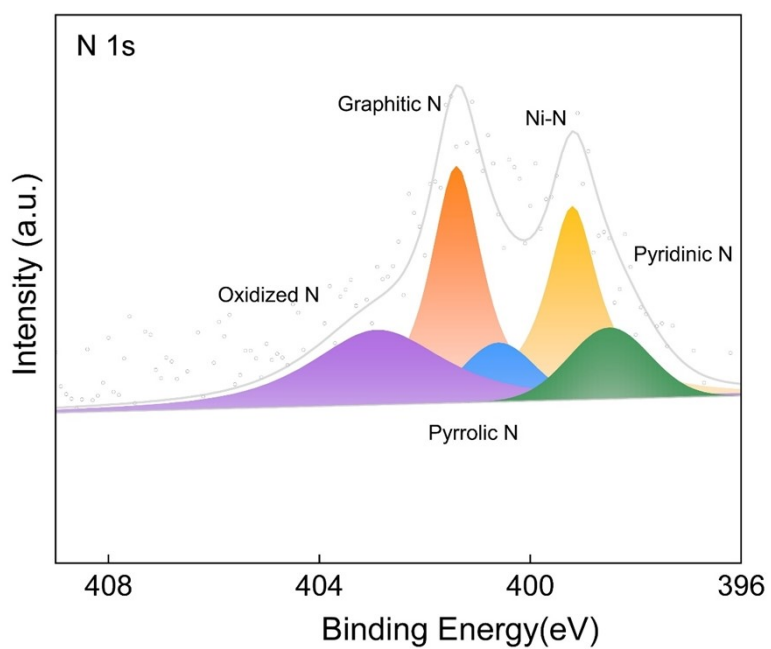


Figure S30. XPS N 1s spectrum of post-catalytic NiNF-1100 in the neutral MEA.

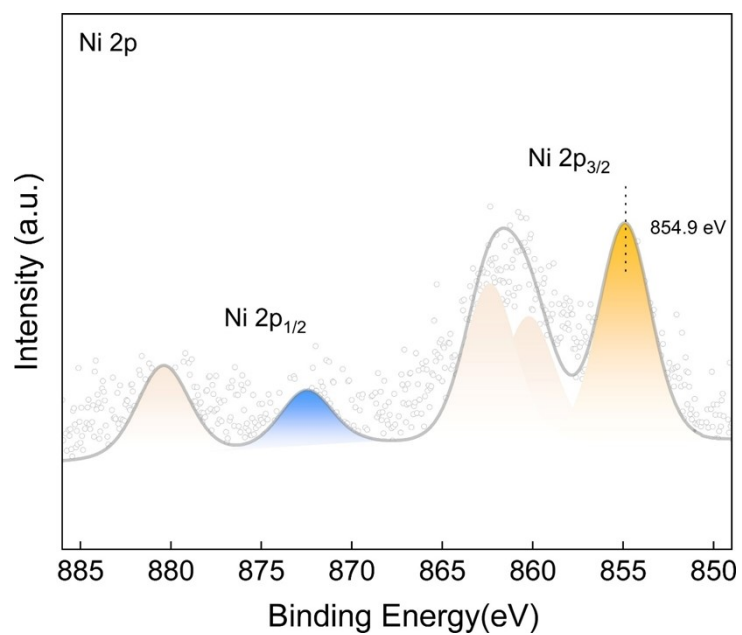


Figure S31. XPS Ni 2p spectrum of post-catalytic NiNF-1100 in the acidic MEA.

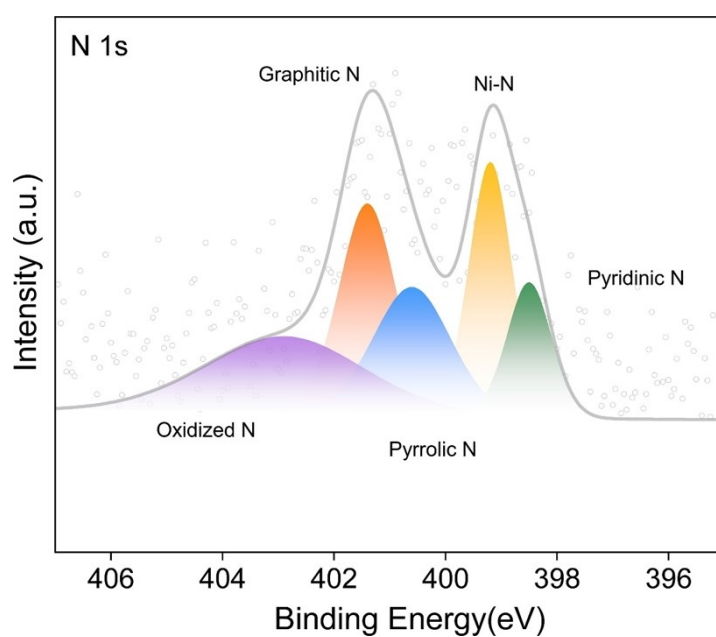


Figure S32. XPS N 1s spectrum of post-catalytic NiNF-1100 in the acidic MEA.

Supporting tables

Table S1. Extended X-ray absorption fine structure fitting parameters at the nickel K-edge.

Sample	Path	S_0^2	CN	R(Å)	ΔE_0 (eV)	σ^2 (Å ²)
NiNF-900	Ni-N	0.85	3.9	1.86	-8.1	0.006
NiNF-1000	Ni-N	0.85	3.8	1.87	-7.0	0.007
NiNF-1100	Ni-N	0.85	3.4	1.85	-10.1	0.008
NiPc	Ni-N	0.85	4	1.85	-9.8	0.009

^aCN is the coordination number; R is interatomic distance (the bond length between Ni central atoms and surrounding coordination atoms); ΔE_0 is edge-energy shift (the difference between the zero kinetic energy value of the sample and that of the theoretical model); σ^2 is Debye-Waller factor (a measure of thermal and static disorder in absorber-scatterer distances).

Table S2. Weight percentages of Ni in different NiNF samples determined by ICP-OES.

Samples	NiNF-900	NiNF-1000	NiNF-1100	Ni-NC
Weight (Ni)%	0.74%	0.72%	0.65%	0.828%
Weight (Zn)%	1.90%	0.26%	0.023%	- [a]

[a] Below detection limit.

Table S3. Summary of CO production efficacy of different electrocatalysts reported in literature.

Catalysts	j_{CO} (mA cm ⁻²)	E (V vs RHE)	Max FE _{CO}	Stability	Ref
Ni-Ga-N	308	-0.91	97%	100 h (300 mA cm ⁻² , Flow cell)	8
Ag-U-mixed	85	3.12 ^[a]	85%	200 h (100 mA cm ⁻² , MEA)	9
Fe-SA/BNC	128.7	3.0 ^[a]	99%	11 h (100 mA cm ⁻² , MEA)	10
AuCuIn/MPL/ CP	270.7	3.2 ^[a]	91.4%	100 h (200 mA cm ⁻² , MEA)	11
NiNCB/ HGTGP	67.5	3.57 ^[a]	90%	103 h (75 mA cm ⁻² , MEA FE _{CO} >83%)	12
NiSA/PCFM	308.4	-1.0	88%	100 h (250 mA cm ⁻² , Flow cell)	13
NiCNC-1000	124.5	-0.8	97.8%	30 h (100 mA cm ⁻² , Flow cell)	1
Co-PPOLs	/	2.7 ^[a]	92%	20 h (180 mA, MEA)	14
NiNF-1100	282 ± 9	-0.5	99.8%	26 h (100 mA cm ⁻² , Flow cell)	This work
	79.76	3.52 ^[a]	99.7%	273 h (400 mA, MEA FE _{CO} >93%)	This work

[a] full-cell voltage.

Table S4. Summary of CO production efficacy of different electrocatalysts in acidic flow cell reported in literature.

Catalysts	j_{total} (mA cm ⁻²)	pH	Max FE _{CO}	Stability(h)	Ref
Au/C	200	4	90%	/	15
Ni-N-C-PTFE	250	2	> 99%	36 h (100 mA cm ⁻²)	16
Au/C	250	0.47	90%	4 h (200 mA cm ⁻²)	17
NiPc-OMe MDE	400	2	>98%	12 h (100 mA cm ⁻²)	18
CoPc-CTF	172.5 ^[a]	2	94.3%	10 h (150 mA cm ⁻²)	19
NiNF-1100	400	2	98%	31 h (100 mA cm ⁻² , FE _{CO} >90%/)	This work

^[a] j_{CO}

Table S5.: Summary of CO production efficacy of different electrocatalysts in neutral or alkaline MEA reported in literature.

Catalysts	j_{CO} (mA cm ⁻²)	Cell Voltage (V)	Max FE _{CO}	Stability	Ref
Ag-U-mixed	85	3.12	85%	200 h (100 mA cm ⁻² , MEA)	9
Fe-SA/BNC	128.7	3.0	99%	11 h (100 mA cm ⁻² , MEA)	10
AuCuIn/MPL/CP	270.7	3.2	91.4%	100 h (200 mA cm ⁻² , MEA)	11
NiNCB/HGTGP	67.5	3.57	90%	103 h (75 mA cm ⁻² , MEA FE _{CO} >83%)	12
Co-PPOLs	/	2.7	92%	20 h (180 mA, MEA)	14
NiNF-1100	79.76	3.52	99.7%	273 h (80 mA cm ⁻² , MEA FE _{CO} >93%)	This work

Table S6. Summary of CO production efficacy of different electrocatalysts in acidic MEA reported in literature.

	SPC _{CO₂} (%)	CO ₂ flow rate (mL min ⁻¹)	j _{total} (mA cm ⁻²)	Max FE _{CO}	Stability	Ref.
Ag	~90%	1	60	40.5%	/	20
	45%	2.5	60	60%	50 h (FE _{CO} >30%)	20
Ni ₅ @NCN	11.8%	30	140	73%	15 h	21
Ni-N-C	77.8%	14.7	500	82%	/	22
	45%	29.5	500	95%	7.5 h	22
NiNF-1100	78%	9.3	320	82% (400 mA)	/	This work
		60	80	97%	18 h (FE _{CO} >65%)	This work

References

- X. Cao, L. Zhao, B. Wulan, D. Tan, Q. Chen, J. Ma and J. Zhang, *Angew. Chem. Int. Ed.*, 2022, **61**, e202113918.
- W. Hua, H. Sun, L. Lin, Q. Mu, B. Yang, Y. Su, H. Wu, F. Lyu, J. Zhong, Z. Deng and Y. Peng, *Chem. Eng. J.*, 2022, **446**, 137296.
- B. Wulan, X. Cao, D. Tan, X. Shu and J. Zhang, *Adv. Funct. Mater.*, 2022, **32**, 2203842.
- W. Ren, X. Tan, W. Yang, C. Jia, S. Xu, K. Wang, S. C. Smith and C. Zhao, *Angew. Chem. Int. Ed.*, 2019, **58**, 6972-6976.
- C. Zhao, X. Dai, T. Yao, W. Chen, X. Wang, J. Wang, J. Yang, S. Wei, Y. Wu and Y. Li, *J. Am. Chem. Soc.*, 2017, **139**, 8078-8081.
- X. Chen, W. Liu, Y. Sun, T. Tan, C. X. Du and Y. Li, *Small Methods*, 2023, **7**, e2201311.
- H. Li, K. Gan, R. Li, H. Huang, J. Niu, Z. Chen, J. Zhou, Y. Yu, J. Qiu and X. He, *Adv. Funct. Mater.*, 2023, **33**, 2208622.
- W. Liu, P. Bai, S. Wei, C. Yang and L. Xu, *Angew. Chem. Int. Ed.*, 2022, **61**, e202201166.
- S. Garg, M. Li, T. Hussain, M. N. Idros, Y. Wu, X. S. Zhao, G. G. X. Wang and T. E. Rufford, *ACS Appl. Mater. Interfaces*, 2022, **14**, 35504-35512.
- J. Luo and X. Liu, *Chem. Eng. J.*, 2022, **437**, 135294.
- G. H. Han, J. Kim, S. Jang, H. Kim, W. Guo, S. Hong, J. Shin, I. Nam, H. W. Jang, S. Y. Kim and S. H. Ahn, *Adv. Sci.*, 2022, **9**, 2104908.
- L. Li, J. Chen, V. S. S. Mosali, Y. Liang, A. M. Bond, Q. Gu and J. Zhang, *Angew. Chem. Int. Ed.*, 2022, **61**, e202208534.
- H. Yang, Q. Lin, C. Zhang, X. Yu, Z. Cheng, G. Li, Q. Hu, X. Ren, Q. Zhang, J. Liu and C. He, *Nat. Commun.*, 2020, **11**, 593.
- W. Zhang, S. Liu, Y. Yang, H. Qi, S. Xi, Y. Wei, J. Ding, Z.-J. Wang, Q. Li, B. Liu and Z. Chen, *Angew. Chem. Int. Ed.*, 2023, **62**, e202219241.

15. M. C. O. Monteiro, M. F. Philips, K. J. P. Schouten and M. T. M. Koper, *Nat. Commun.*, 2021, **12**, 4943.
16. X. Sheng, W. Ge, H. Jiang and C. Li, *Adv. Mater.*, 2022, **34**, 2201295.
17. J. Gu, S. Liu, W. Y. Ni, W. H. Ren, S. Haussener and X. L. Hu, *Nat. Catal.*, 2022, **5**, 268-276.
18. Z. Jiang, Z. Zhang, H. Li, Y. Tang, Y. Yuan, J. Zao, H. Zheng and Y. Liang, *Adv. Energy Mater.*, 2023, **13**, 2203603.
19. Q. Wu, D. H. Si, J. Liang, Y. B. Huang and R. Cao, *Appl. Catal. B*, 2023, **333**, 122803.
20. B. Pan, J. Fan, J. Zhang, Y. Luo, C. Shen, C. Wang, Y. Wang and Y. Li, *ACS Energy Lett.*, 2022, **7**, 4224-4231.
21. Z. Liu, T. Yan, H. Shi, H. Pan, Y. Cheng and P. Kang, *ACS Appl. Mater. Interfaces*, 2022, **14**, 7900-7908.
22. H. Li, H. Li, P. Wei, Y. Wang, Y. Zang, D. Gao, G. Wang and X. Bao, *Energy Environ. Sci.*, 2023, **16**, 1502-1510.